Updating the model of a rotor with surface mounted permanent magnets in an active magnetic bearing rotor system

Jouni VUOJOLAINEN*, Alexander SMIRNOV*, Rafal JASTRZEBSKI*, Teemu SILLANPÄÄ*, Behnam GHALAMCHI**, Toni HARTIKAINEN*** and Olli PYRHÖNEN*

*Dept. of Electrical Engineering, **Dept. of Mechanical Engineering, Lappeenranta University of Technology

Skinnarilankatu 34, 53850 Lappeenranta, Finland

E-mail: Jouni.Vuojolainen@lut.fi

***Aurelia Turbines

Laserkatu 6, 53850 Lappeenranta, Finland

Abstract

In this publication, the finite element method (FEM) model of a rotor of permanent magnet (PM) machine with surface mounted permanent magnets is updated. Typically rotors are modeled with FEM, but the model is still only an approximation of the real rotor. The rotor is constructed from number of different elements and have a complex geometry. Electrical machine part might have slits, surface mounted or embedded permanent magnets. Elements are often connected with shrink fits and this leads to the properties discrepancy compared to the elements described with Timoshenko beam theory. In the work, specific elements are selected as uncertain based on engineering experience and the elasticity values of these elements is updated. Experimental data is obtained with AMB system identification and then the frequency difference in the resonance and anti-resonance frequencies between the experimental data and FEM-model is minimized. When the frequency difference has been minimized, the updated FEM-model corresponds better to the experimental data. The updated model is utilized for controller synthesis procedure to improve performance of the control system. An AMB PM machine with surface mounted permanent magnets was used to test the rotor model update procedure. The procedure allowed to fit the model to the experimental data with accuracy of 56.57 %.

Keywords : System identification, Frequency response function (FRF), Active magnetic bearing (AMB), Finite element method (FEM), Permanent magnet (PM), Rotor model update

1. Introduction

In high-speed electrical machines one of the possible bearing solution are active magnetic bearings (AMBs). The absence of contact, lubrication freeness, and reduced maintenance makes these bearing quite attractive. In addition as magnetic bearings include sensors it makes easy to implement process monitoring and identification in the system.

For high-speed applications, different types of electrical machines are used. An induction machine with the solid rotor can provide a robust solution. The main drawback is low power factor. To overcome this issue the rotor can be coated or slitted, in addition end-rings can be used. The slitted rotor is convenient solution because of the ease of manufacturing such a structure (Pyrhönen, et al., 2009). Slits in general are used to tune the performance of the rotor and the full machine (Yetgin and Turan, 2014; Pyrhönen, et al., 2009). Permanent magnet (PM) machines on the other hand have a high efficiency and high power factor and is the reason to utilize PM machines. PM machines are also suited for variable speed applications (Belachen and Arkkio, 2010).

Modern AMBs utilize model-based controllers to stabilize the system (Maslen and Sawicki, 2007). To obtain such controllers an accurate model of the rotor is necessary and desirably with low number of states to reduce the order of the controller. Rotors used in high-speed applications with AMBs are modeled with finite element method (FEM). A

common approach is to utilize beam elements and discretize the rotor only along its axial dimension (Genta, 2005). The full 3D FEM modelling is quite computationally expensive and provides comparable results to 1D model. To take into account the flexibility in Timoshenko beam theory the elasticity behavior of material and its Poisson's ratio are necessary (Lösch, 2002).

The FEM-model of the rotor is still only an approximation of the real rotor. Real rotors have a complex geometry and are constructed from number of different components, which are connected with shrink fits, hirth couplings, shaft collars and several other methods. All these uncertainties lead to the properties discrepancy compared to the elements described with Timoshenko beam theory. Especially the electrical machine part might have a complex geometry with slits, surface mounted or embedded permanent magnets. In PM machines modeling the surface mounted permanent magnets is difficult (Faustner, et al., 2015; Belachen and Arkkio, 2010). Modeling PM machines with embedded permanent magnets is even more difficult (Han, et al., 2007).

To update the FEM-model of the rotor authors in (Wróblewski, et al., 2012) present a method which uses resonance and anti-resonance frequency information from model and experimental data obtained with AMB system identification. With this method, frequency difference in the resonance and anti-resonance frequencies between the experimental data and model data is minimized. Some elements in the FEM-model are selected as uncertain based on engineering experience. The elasticity value of these elements is tuned to minimize the mentioned difference between experimental data and model data. Minimization in this case is done with the well-known Nelder-Mead method (Nelder and Mead, 1965).

The application of the above mentioned method to the PM machines with surface mounted permanent magnets is not presented in the literature. Thus this paper contributes by analyzing and updating the rotor model of an AMB PM machine with surface mounted permanent magnets.

The paper is constructed as follows. First FEM-modeling, AMB system identification and the rotor model update method are discussed. Then the rotor structure is presented and the locations of the uncertain elements are presented. Next, the FEM-model of the rotor is updated. Finally results are provided by comparing the nominal FEM-model of the rotor and the updated FEM-model with experimental identification data.

Nomenclature

$B(\boldsymbol{e})$	black box function, error function
DX	drive end x-axis
e_p	design variable, elasticity value of the p:th uncertain element
$\boldsymbol{e}$	design variable vector
err_{DX}	error in the drive end x-axis (DX)
err_{NX}	error in the non-drive end x-axis (NX)
err_{tot}	total error
$f_k^{a,\mathrm{E}}$	anti-resonance frequency error
$f_k^{\mathrm{r,E}}$	resonance frequency error
k	index of flexible mode
k_t	total number of flexible modes per one axis
n	number of design variables
NX	non-drive end x-axis
$\widehat{\omega}_k^{\mathrm{a}}$	anti-resonance frequency from experimental data
$\widetilde{\omega}_k^{\mathrm{a}}$	anti-resonance frequency from model
$\widehat{\omega}_k^{\mathrm{r}}$	resonance frequency from experimental data
$\widetilde{\omega}_k^{r}$	resonance frequency from model
w_k	weight of the k:th flexible mode

2. Methods

In this section FEM-modeling of the rotor, AMB system identification, and the rotor model update method are discussed.

2.1 Finite element method modeling

In this case study, flexible rotor is model using FEM. FEM-methods are well developed and have been utilized in rotor dynamics for over two decades (Shiau and Hwang, 1989; Genta, 2005; Friswell, et al., 2010).

Because rotors are usually axisymmetric in the *xy*-plane they are modeled with cylinders. Timoshenko beam theory is used to describe the cylinders. With Timoshenko beams, the rotational inertia is taken into account and also the shear deformation (Smirnov, 2012). Elasticity behavior of material and its Poisson's ratio are necessary to take into account the flexibility in the Timoshenko beam theory (Lösch, 2002).

2.2 AMB system identification

AMBs are equipped with both sensors and actuators, it makes possible to excite the system and measure the response. Although in general the system works in closed-loop with controller by accepting some assumptions it is possible to extract accurate enough response of the open-loop part (Schweitzer and Maslen, 2009). With AMB system identification, the frequency response of the experimental rotor-bearing system is obtained. In this case an adaptive amplitude stepped sine signal is used. Amplitude of the sine wave is adjusted in order to get an acceptable response. The value of the position displacement (response) for the exited axis is kept between two limits in this case 20 µm and 50 µm. If response is lower than 20 µm amplitude is increased by 20% and if response is higher than 50 µm amplitude is decreased by 20 % respectively. When response is between these limits, it's acceptable, identification data is saved and the next frequency is selected. Amplitude range is from 50 mA to 2.5 A. Also if amplitude is less than 50 mA or greater than 2.5 A, identification data is saved and next frequency is selected. Three different frequency bands were used. First frequency band was from 1 Hz to 97.89 Hz in 12.11 Hz steps (9 points), second frequency band was from 100 Hz to 700 Hz in 2.41 Hz steps (250 points) and the third from 703.44 Hz to 1200 Hz in 12.11 Hz steps (42 points).

The experimental data is then used to make a parametric model of the rotor with least squares optimization. From this parametric model, resonance and anti-resonance frequencies are extracted.

2.3 Rotor model update method

FEM-modeling of the rotor has limitations, and makes only an approximation of the rotor. Modeling complex geometries and connections between different elements with shrink fits is difficult. Also the modeling of the electrical machine part is hard as there might be embedded or surface mounted permanent magnets or slits. Thus Timoshenko beam theory is unable to describe fully the properties of these complex elements. These complex elements are selected as uncertain and their properties are updated.

Authors in (Wróblewski, et al., 2012) present a method to update the FEM-model of the rotor. In this method, the frequency difference in the resonance and anti-resonance frequencies between the experimental data and FEM-model data is minimized. Experimental data is obtained as discussed in section 2.2. From the FEM-model, some uncertain elements are selected and the elasticity values of these elements is updated in order to minimize the frequency difference in the resonance and anti-resonance frequencies between the experimental data and FEM-model of the rotor. All other elasticity values and the material properties remained at the fixed nominal values.

Elasticity value of an uncertain element is denoted with design variable e_p. All design variables e_p are combined in to a design variable vector $\boldsymbol{e}$ (Wróblewski, et al., 2012)

$$\boldsymbol{e} \in \mathbb{R}^{\boldsymbol{n}} \text{ so that } \quad \{e_p\}_{p=1\ldots n}, \tag{1}$$

where n is the number of design variables. The design variable vector $\boldsymbol{e}$ is used to calculate a new FEM-model of the rotor based on the changed elasticity values e_p.

After obtaining a new model with the design variable vector $\boldsymbol{e}$, resonance and anti-resonance frequencies are extracted for the selected axes and compared with the resonance and anti-resonance frequencies obtained with experimental data. Errors are calculated separately for resonance and anti-resonance frequencies using relative errors. The errors are weighted and the weight is the same for all axes but different for each flexible mode. In this case two axes are used, drive end *x*-axis (DX) and non-drive end *x*-axis (NX). If resonances on both DX-axis and NX-axis are used on the same flexible mode in the error calculation, the weight is halved for these resonances in order to prevent over-representation of the resonance errors compared to the anti-resonance errors. Variable $f_k^{r,\mathrm{E}}$ is used to represent the

resonance frequency error for one axis on the k:th flexible mode, $f_k^{a,\mathrm{E}}$ is used to represent the anti-resonance frequency error and weights are represented with w_k. These errors are then calculated with (adapted from Wróblewski, et al., 2012)

$$f_k^{\mathrm{r,E}} = w_k \frac{|\hat{\omega}_k^{\mathrm{r}} - \tilde{\omega}_{,k}^{\mathrm{r}}|}{\hat{\omega}_k^{\mathrm{r}}} \text{ and} \quad (2)$$

$$f_k^{\mathrm{a,E}} = w_k \frac{|\hat{\omega}_k^{\mathrm{a}} - \tilde{\omega}_k^{\mathrm{a}}|}{\hat{\omega}_k^{\mathrm{a}}}, \quad (3)$$

where $\hat{\omega}_k^{\mathrm{r}}$ is the experimental resonance frequency, $\tilde{\omega}_k^{\mathrm{r}}$ is the resonance frequency obtained from the FEM-model, $\hat{\omega}_k^{\mathrm{a}}$ is the anti-resonance frequency from experimental data, $\tilde{\omega}_k^{\mathrm{a}}$ is the anti-resonance frequency obtained from the FEM-model. These errors are then calculated for the selected axes and flexible modes. Error on DX- and NX-axis is calculated with

$$err_{\mathrm{DX}} = \sum_{k=1}^{k_{\mathrm{t}}} \left(f_k^{\mathrm{r,E}} + f_k^{\mathrm{a,E}} \right) \text{ and} \quad (4)$$

$$err_{\mathrm{NX}} = \sum_{k=1}^{k_{\mathrm{t}}} \left(f_k^{\mathrm{r,E}} + f_k^{\mathrm{a,E}} \right), \quad (5)$$

where k_{t} is the total number of flexible modes per one axis. Total error value is obtained by summing the error on DX- and NX-axis

$$err_{\mathrm{tot}} = err_{\mathrm{DX}} + err_{\mathrm{NX}}. \quad (6)$$

Equation (6) shows the error function we try to minimize.

A black box function $B(\boldsymbol{e})$ is formulated to describe the process of determining the FEM-model based on value of the design variable vector $\boldsymbol{e}$ and outputting the total error value. Function to be minimized is then generalized as (Wróblewski, et al., 2012)

$$\min_{e \in \mathbb{R}^n} B(\boldsymbol{e}). \quad (7)$$

Minimization of Eq. (7) is done with the well-known Nelder-Mead function minimization method (Nelder and Mead, 1965).

3. Experiments and Results

A five degree-of-freedom AMB PM machine with surface mounted permanent magnets was used to test the rotor model update method presented in section 2.3. The machine has two radial and one axial active magnetic bearing. Machine's FEM-model of the rotor is shown in Fig. 1. Design variables locations e_p are also shown in Fig. 1.

Design variables ($e_1 \ldots e_6$) are located at the generator magnets. These generator magnets are considered as a ring on top of the electrical machine part of the shaft. In the real machine the length of the generator is covered by small magnets, which are tightened to the shaft and in practice should not apply high stiffness to the shaft. Thus, nominal elasticity value of these design variables was 2.2 GPa (~1% of steel elasticity 211 GPa).

Design variables ($e_7 \ldots e_{12}$) are located at the electrical machine part of the shaft (under the generator magnets). Nominal elasticity value of these design variables was 211 GPa.

Design variables ($e_{13} \ldots e_{15}$) are located at the part of the shaft where impeller is connected. Nominal elasticity value of these design variables was assumed to be also 211 GPa.

Design variable e_{16} is located at the outer part of the non-drive end AMB and design variable e_{17} is located at the outer part of the drive end AMB respectively. These outer parts of the AMBs are also considered as a ring and represent the laminations. Laminations are constructed from thin cut steel which is then pressed together and tightened to the shaft and should not also apply high stiffness to the shaft. Nominal elasticity value of these design variables was 2.1 GPa (~1% of steel elasticity 211 GPa).

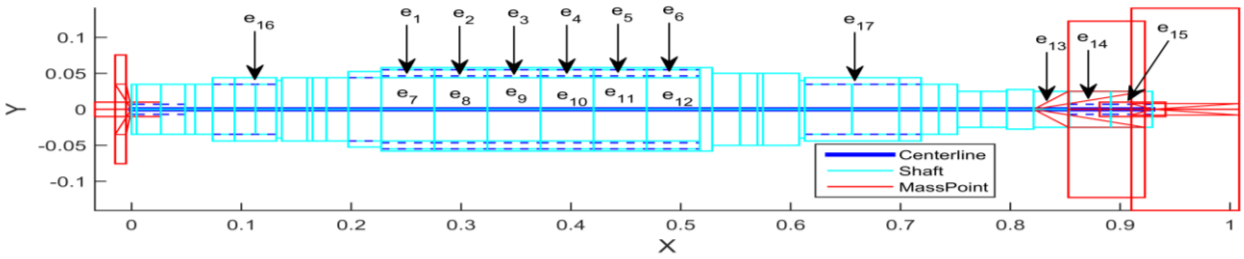

Fig. 1 FEM-model of the machine's rotor. Design variable locations e_p shown.

3.1 Rotor model update

FEM-model of the rotor was then updated with the method shown in section 2.3. In the update routine first, second and third resonance and anti-resonance frequencies were used on the DX-axis and first and second resonance and anti-resonance frequencies on the NX-axis respectively. Third resonance and anti-resonance frequencies on the NX-axis were not used because they were not visible in the experimental data, which is presented in Fig. 2. First flexible modes were weighted with 1, second modes with 0.5 and third modes with 0.25. This weighting was used because the lower flexible modes are more important to fit than the higher ones and because the beam elements are good to predict the first and second modes. Comparison between the DX- and NX-axis resonance and anti-resonance frequencies of the experimental data, nominal FEM-model and the updated FEM-model is shown in Table 1.

Table 1 Comparison between the resonance and anti-resonance frequencies on the DX- and NX-axis between the experimental data, nominal and updated FEM-model of the rotor.

Feature of interest	Experimental data [Hz]	Nominal model [Hz]	Absolute error [Hz]/(%)	Updated model [Hz]	Absolute error [Hz]/(%)
1st Resonance DX/NX	237.00	231.47	5.53 / (2.32)	233.91	3.09 / (1.31)
1st Anti-resonance DX	160.00	164.67	4.67 / (2.92)	165.81	5.81 / (3.63)
1st Anti-resonance NX	204.00	201.54	2.46 / (1.20)	204.00	0.00 / (0.00)
2nd Resonance DX	613.00	563.98	49.02 / (8.00)	617.20	4.20 / (0.69)
2nd Resonance NX	616.00	563.98	52.02 / (8.45)	617.20	1.20 / (0.20)
2nd Anti-resonance DX	543.00	501.14	41.86 / (7.71)	542.99	0.01 / (0.00)
2nd Anti-resonance NX	601.00	546.64	54.36 / (9.05)	600.97	0.03 / (0.01)
3rd resonance DX	1006.00	937.57	68.43 / (6.80)	1020.60	14.61 / (1.45)
3rd Anti-resonance DX	897.00	796.39	100.61 / (11.22)	884.82	12.18 / (1.36)

Table 1 shows, that the nominal model of the rotor matches the experimental data quite accurately on the first resonance and anti-resonance frequency, maximum absolute error being only 5.53 Hz. On the second flexible mode, the maximum absolute error is 54.36 Hz. The third resonance and anti-resonance frequency on the DX-axis has maximum absolute error of 100.61 Hz.

The updated model has a slightly bigger error on the first flexible mode compared to the nominal model, maximum absolute error value being 5.81 Hz. Second resonance and anti-resonance frequency fit on the updated model has improved and the maximum absolute error is only 4.2 Hz. The third DX-axis flexible mode has improved the most, maximum absolute error being 14.61 Hz.

Figure 2 shows the frequency response functions (FRFs) of the experimental data, nominal model and the updated model of the rotor on DX- and NX-axis.

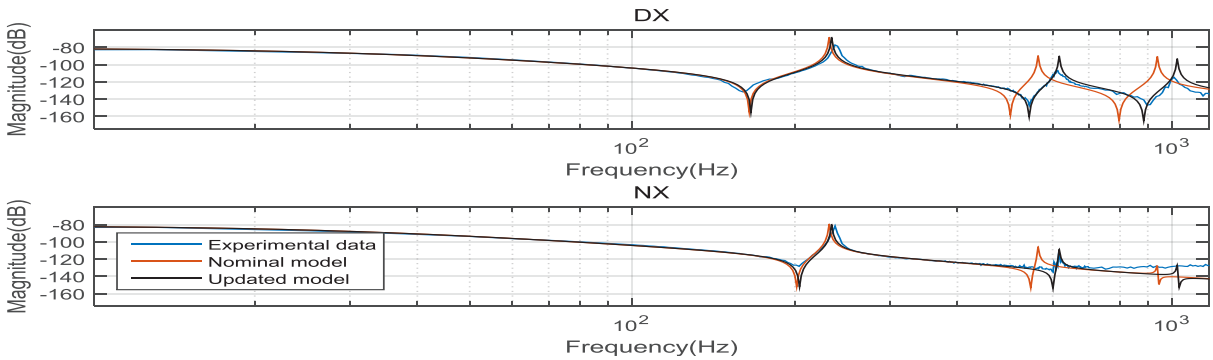

Fig. 2 Frequency response functions of the experimental data, nominal model and updated model of the rotor on DX- and NX-axis.

From Fig. 2 it can be seen that the updated model fits better with the experimental data. Also on the NX-axis the third flexible mode can't be seen. Figure 3 shows the updated elasticity e_p from the updated model and Fig. 4 shows the difference between the elasticity values of the nominal and updated model in percent.

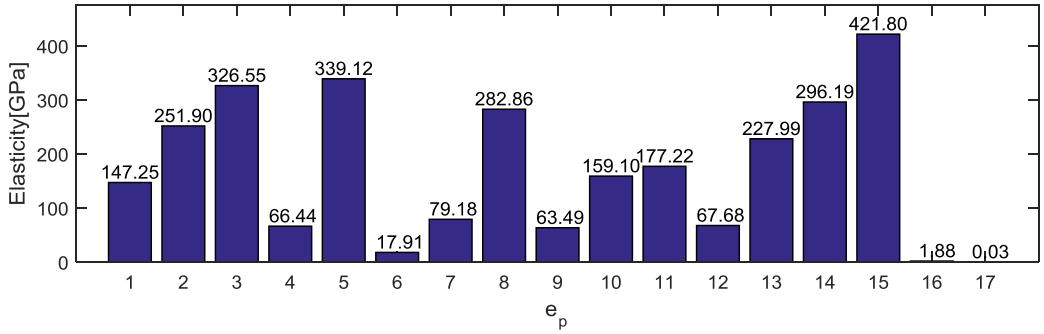

Fig. 3 Updated elasticity values e_p from the updated FEM-model of the rotor. Elasticity value of e_{16} is 1.88 GPa and elasticity value of e_{17} is 25.29 MPa.

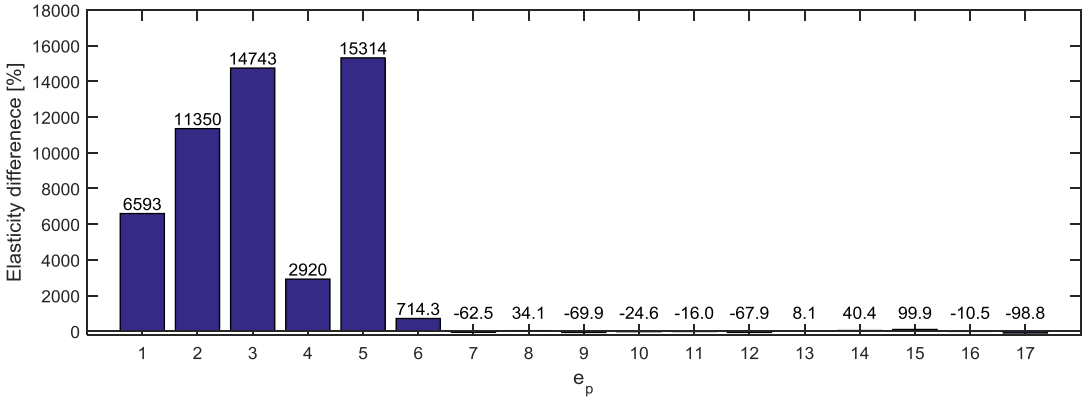

Fig. 4 Elasticity difference between the nominal and updated elasticity value e_p in percent.

Figure 4 shows that elasticity values of the generator magnets ($e_1 \ldots e_6$) have increased from the nominal value of 2.2 GPa. Also it can be noted that there are quite high variation (14 600%) between these updated elasticity values. One reason of this might be the difficulty to model the embedded permanent magnets.

Secondly, elasticity values of the electrical machine part of the rotor shaft ($e_7 \ldots e_{12}$) other than the value of e_8 have decreased from the nominal value of 211 GPa. The probable reason for this are the cooling channels creating slits in the rotor shaft. Variation of these stiffness values is 104 %.

Thirdly, on the part of the rotor shaft where impeller is connected ($e_{13} \ldots e_{15}$), these elasticity values have increased from the nominal value of 211 GPa. Elasticity value of e_{13} (227.99 GPa) is quite close to the nominal value. Reason for this increase is the additional stiffness from the impeller at the point of connection to the rotor shaft. Although the impeller is modeled as point mass it might add some stiffness when its axial length is big enough and tight fitting is applied. Variation of these elasticity values is 91.9 %.

Fourthly, elasticity values of the drive and non-drive end outer part of the AMB (e_{16} and e_{17}) have decreased from the nominal value of 2.1 GPa. The nominal and the updated elasticity value of these elements is small and thus has very little effect on the resonance and anti-resonance frequencies. In general the lamination stacks are characterized by reduced stiffness. Variation of these elasticity values is 88.3 %.

Figure 5 shows how the output of the error function $B(\boldsymbol{e})$ changes during each iteration step in the rotor model update method. In ideal case output of the $B(\boldsymbol{e})$ would converge to 0, but in practice it converges to some value depending on the starting elasticity values e_p.

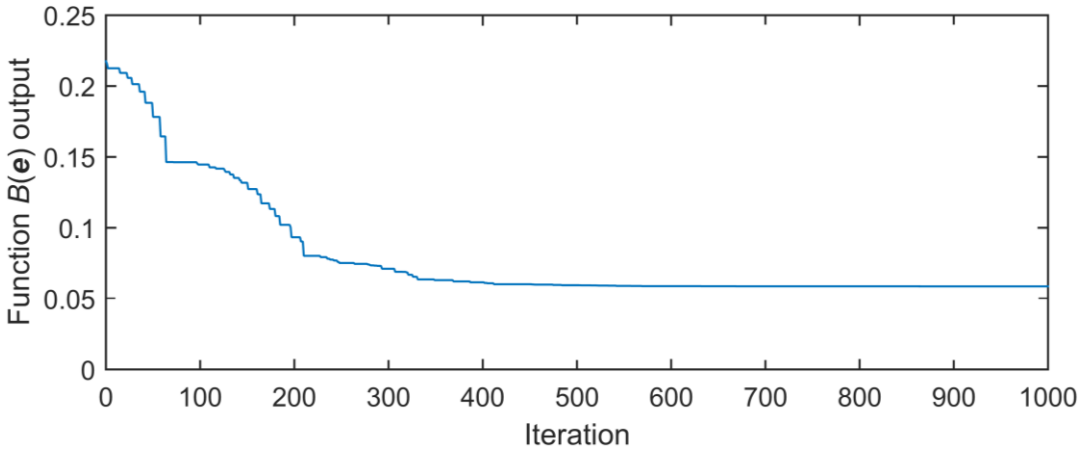

Fig. 5 Output of the error function $B(\boldsymbol{e})$ during the machine's rotor model update.

From Fig. 5 it can be noted, that during the first 65 iterations, the B($\boldsymbol{e}$) output decreases rapidly. The next major decrease points can be noted at around 210 followed by the point at 330 iterations. At around 500 iterations, the B($\boldsymbol{e}$) output starts to converge and only minimal improvement is achieved in the later iteration steps. Running one rotor model update with 1000 iterations takes about 52 seconds. The runtime is dependent on how many function evaluations are needed during the Nelder-Mead function minimization.

4. Conclusion

Timoshenko beam element was used to model the flexible rotor with surface mounted permanent magnets. In preliminary model, some random elasticity values was picked for uncertain elements such as generator and AMB lamination and impeller fittings. Comparing with measurement results, preliminary analysis show significant error, especially in higher modes. Rotor model was updated using Nelder-Mead method with changing elasticity values which matches better the resonance and anti-resonance frequencies of the experimental data. Results show that the rotor model is more sensitive in generator magnets properties. In some case, the updated elasticity is 150 times higher than original estimation. Another interesting point in analysis in e_{15} where the impeller is connected to the shaft and 100% higher elasticity is needed for updated model. It is also important to consider the difference between AMB laminations in D-end and ND-end where the D-end lamination illustrates need to update with original. The reason can be the mass properties of the whole shaft which is near to D-end bearing because of the impeller attachment.

In general, the updated model is more accurate in first three natural frequencies compared with experimental data's and the total model fit of the updated model was 56.57 % compared to the nominal fit of 30.63%.

Acknowledgment

The work has been partially supported by Academy of Finland, decisions No. 270012 and No. 273489.

References

Belachen, A. and Arkkio, A., Permanent magnets models and losses in 2D FEM simulation of electrical machines, XIX International Conference on Electrical Machines (ICEM) (2010), pp.1-6.

Faustner, D., Kemmetmüller, W. and Kugi, A., Magnetic equivalent circuit modeling of a saturated surface-mounted permanent magnet synchronous machine, 8th Vienna International Conference on Mathematical Modelling (MATHMOD) (2015), IFAC-PapersOnLine, Vol.48, Issue 1 (2015), pp.360-365.

Friswell, M. I., Penny, J. E. T., Garvey, S. D. and Lees A. W., Dynamics of Rotating Machines (2010), Cambridge University Press.

Genta, G., Dynamics of Rotating Systems (2005), New York, NY: Springer US.

Han, S.-H., Jahns, T. M. and Soomg, W. L., A magnetic circuit model for and IPM synchronous machine incorporating

moving airgap and cross-coupled saturation effects, IEEE International Electric Machines & Drives Conference, Vol.1 (2007), pp.21-26.

Lösch, F., Identification and automatic controller design for active magnetic bearing systems (2002), Doctoral Thesis ETH Zürich, Switzerland.

Maslen, E. H. and Sawicki, J. T., Mu-synthesis for magnetic bearings: why use such a complicated tool?, Mechanical Systems and Control Parts A, B, C, Vol.9 (2007), pp.1103–1112.

Nelder, J. A. and Mead, R., A simplex method for function minimization, The Computer Journal (1965), pp.308-313.

Pyrhönen, J., Nerg, J., Mikkola, A., Sopanen, J. and Aho, T., Electromagnetic and mechanical design aspects of a high-speed solid-rotor induction machine with no separate copper electric circuit in the megawatt range, Electr. Eng., Vol.91, No.1 (2009), pp.35–49.

Schweitzer, G. and Maslen, E. H., Magnetic Bearings (2009), Berlin, Heidelberg: Springer Berlin Heidelberg.

Shiau, T. N. and Hwang, J. L., A new approach to the dynamic characteristic of undamped rotor-bearing systems, Journal of Vibration, Acoustics, Stress, and Reliability in Design, Transactions of the ASME, Vol.111, Issue 4 (1989), pp.379-385.

Smirnov, A., AMB system for high-speed motors using automatic commissioning (2012), Doctoral Thesis, Lappeenranta University of Technology, Finland.

Wróblewski, A. C., Sawicki, J. T. and Pesch, A. H., Rotor model updating and validation for an active magnetic bearing based high-speed machining spindle, Journal of Engineering for Gas Turbines and Power, Transactions of the ASME, Vol.134, Issue 12 (2012), pp.122509.

Yetgin, A. G., and Turan, M., Effiency optimization of slitted-core induction motor, Journal of Electrical Engineering, Vol.65, No.1 (2014), pp.60-64.